JACS Au
AN OPEN ACCESS JOURNAL OF THE AMERICAN CHEMICAL SOCIETY

pubs.acs.org/jacsau

Article

Uncovering the CO_2 Capture Mechanism of $NaNO_3$-Promoted MgO by ^{18}O Isotope Labeling

Annelies Landuyt, Priyank V. Kumar, Jodie A. Yuwono, Alexander H. Bork, Felix Donat, Paula M. Abdala, and Christoph R. Müller*

Cite This: *JACS Au* 2022, 2, 2731−2741

Read Online

ACCESS | Metrics & More | Article Recommendations | Supporting Information

ABSTRACT: MgO-based CO_2 sorbents promoted with molten alkali metal nitrates (e.g., $NaNO_3$) have emerged as promising materials for CO_2 capture and storage technologies due to their low cost and high theoretical CO_2 uptake capacities. Yet, the mechanism by which molten alkali metal nitrates promote the carbonation of MgO (CO_2 capture reaction) remains debated and poorly understood. Here, we utilize ^{18}O isotope labeling experiments to provide new insights into the carbonation mechanism of $NaNO_3$-promoted MgO sorbents, a system in which the promoter is molten under operation conditions and hence inherently challenging to characterize. To conduct the ^{18}O isotope labeling experiments, we report a facile and large-scale synthesis procedure to obtain labeled MgO with a high ^{18}O isotope content. We use Raman spectroscopy and *in situ* thermogravimetric analysis in combination with mass spectrometry to track the ^{18}O label in the solid ($MgCO_3$), molten ($NaNO_3$), and gas (CO_2) phases during the CO_2 capture (carbonation) and regeneration (decarbonation) reactions. We discovered a rapid oxygen exchange between CO_2 and MgO through the reversible formation of surface carbonates, independent of the presence of the promoter $NaNO_3$. On the other hand, no oxygen exchange was observed between $NaNO_3$ and CO_2 or $NaNO_3$ and MgO. Combining the results of the ^{18}O labeling experiments, with insights gained from atomistic calculations, we propose a carbonation mechanism that, in the first stage, proceeds through a fast, surface-limited carbonation of MgO. These surface carbonates are subsequently dissolved as $[Mg^{2+}\cdots CO_3^{2-}]$ ionic pairs in the molten $NaNO_3$ promoter. Upon reaching the solubility limit, $MgCO_3$ crystallizes at the MgO/$NaNO_3$ interface.

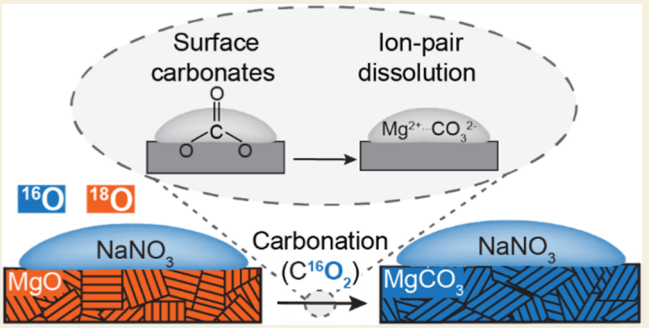

KEYWORDS: *CO_2 capture, MgO sorbents, ^{18}O isotope labeling, density functional theory (DFT), Raman spectroscopy, molten salts*

INTRODUCTION

Carbon dioxide is one of the major greenhouse gases contributing to global warming.[1] Carbon dioxide capture, utilization, and storage technologies offer solutions for the reduction of anthropogenic CO_2 emissions into the atmosphere.[2,3] Currently, aqueous amine solutions are the benchmark technology for CO_2 capture on the industrial scale.[4−6] However, amine scrubbing processes feature some disadvantages, including a high energy penalty for the release of CO_2 (due to large water content), a low temperature of operation during the CO_2 capture process (requiring a precooling of the gas stream in the case of precombustion or postcombustion capture[7,8]) and the oxidative degradation of the amines during cyclic operation.[9,10] Therefore, the development of CO_2 sorbents that show low costs per ton of CO_2 captured, high cyclic stability, and high gravimetric CO_2 uptake is a very active research area. In this context, solid CO_2 sorbents, for example, porous adsorbents such as zeolites, metal organic frameworks, activated carbons, or CO_2-absorbing materials such as metal oxides, are promising candidates.[11−15] Alkaline earth metal oxides, such as MgO or CaO, react stoichiometrically with CO_2 and have therefore high theoretical uptake capacities of 1.09 and 0.79 $g_{CO_2}/g_{sorbent}$, respectively.[11] The high theoretical uptake capacity of MgO in combination with its low cost and the comparatively low energy requirement for regeneration makes it a promising CO_2 sorbent material for operation in the intermediate temperature range (250−450 °C).[16] The reversible carbonation reaction of MgO proceeds as follows

$$MgO(s) + CO_2(g) \rightleftharpoons MgCO_3(s) \quad (1)$$

Despite its high theoretical uptake capacity, the reported CO_2 uptake capacities of MgO have been significantly lower, that is, in the range <0.2 $g_{CO_2}/g_{sorbent}$.[17−19] This limited CO_2

Received: August 22, 2022
Revised: November 17, 2022
Accepted: November 18, 2022
Published: December 1, 2022

https://doi.org/10.1021/jacsau.2c00461
JACS Au 2022, 2, 2731−2741

uptake has been attributed to both the high lattice enthalpy of MgO and the formation of a dense layer of surface carbonates upon carbonation, acting as a self-limiting layer against further carbonation.[20,21] To circumvent some of these limitations, alkali metal nitrates, for example, $NaNO_3$, which are molten under operating conditions have been introduced as promoters, boosting the conversion of MgO to values of up to 75%.[22] Despite the efficacy of molten salt promoters, the actual promotion mechanism remains highly debated.[16,22−26]

So far, a series of promotion mechanisms have been proposed. For instance, Zhang et al. reported that the role of the molten alkali metal nitrate salt is to dissolve bulk MgO, yielding $[Mg^{2+}\cdots O^{2-}]$ ion pairs in the molten nitrate salt. CO_2 adsorbs on the bare MgO surface and reacts with the dissolved ion pairs at the triple phase boundary of MgO, $NaNO_3$, and CO_2.[22] In contrast, Harada et al. suggested that the role of the promoter is to dissolve CO_2 and thereby prevent the formation of an impermeable layer of surface carbonates.[24] The dissolved CO_2 immediately reacts with oxide ions that originate from the dissociation of the nitrate group to form carbonate ions. In the reaction scheme proposed by Harada et al., the formation of $MgCO_3$ takes place at the MgO/$NaNO_3$ interface. Experimental evidence of the nucleation and growth of $MgCO_3$ at the liquid−solid interfaces has been recently provided by X-ray- and electron microscopy-based techniques, revealing that the nucleation sites are located at the buried MgO/$NaNO_3$ interface.[27,28] Furthermore, Bork et al. observed the presence of etching pits on the surface of a carbonated MgO single crystal in the proximity of $MgCO_3$, providing evidence that $MgCO_3$ forms via a dissolution−recrystallization mechanism.[27]

To develop further MgO-based sorbents for CO_2 capture, it is critical to elucidate the key intermediate steps in the carbonation reaction of alkali metal nitrate-promoted MgO. In this context, isotope labeling is a useful technique to unravel reaction mechanisms as it allows to trace atoms during reactions.[29−36] Recently, Gao et al. have used ^{18}O labeling to investigate the carbonation mechanism of $NaNO_3$-promoted MgO.[37] Based on transient ^{18}O isotopic exchange experiments using ^{18}O-labeled $NaNO_3$, the authors propose that the molten salt actively participates in the carbonation reaction by dissociating into NO_2^+ and O^{2-}. In our study, we introduce an ^{18}O label into CO_2, MgO, or $NaNO_3$ and trace the ^{18}O label by Raman spectroscopy and *in situ* thermogravimetric analysis (TGA) in combination with mass spectrometry (MS) and atomistic calculations. Our experimental work provides evidence for a rapid oxygen exchange between CO_2 and MgO at the surface of MgO, through the formation of surface carbonates, prior to bulk $MgCO_3$ formation. This oxygen exchange reaction occurs both on unpromoted and $NaNO_3$-promoted MgO, indicating the highly dynamic nature of surface carbonates, also in the absence of a promoter. Furthermore, using a combination of TGA−MS and Raman spectroscopy, we demonstrate that the oxygen atoms of the nitrate group of $NaNO_3$ do not participate in the carbonation reaction at 315 °C (typical carbonation temperature). Combining our experimental observations with density functional theory (DFT) and ab initio molecular dynamics (AIMD) modeling, we propose a mechanism in which a fast surface carbonation of MgO is followed by ion-pair dissolution of surface carbonates into the molten salt and their subsequent crystallization as bulk $MgCO_3$ at the MgO/$NaNO_3$ interface.

RESULTS AND DISCUSSION

Structural and Surface Characterization of the Synthesized MgO and $Mg^{18}O$ Sorbents

We have developed a facile synthesis route to yield ^{18}O-labeled MgO nanoparticles by reacting Mg_3N_2 with ^{18}O-labeled water, followed by vacuum treatment at 700 °C to transform the formed $Mg(^{18}OH)_2$ into $Mg^{18}O$. Unlabeled MgO was prepared via the same route by replacing ^{18}O-labeled water with standard deionized water. Figure 1 plots the XRD

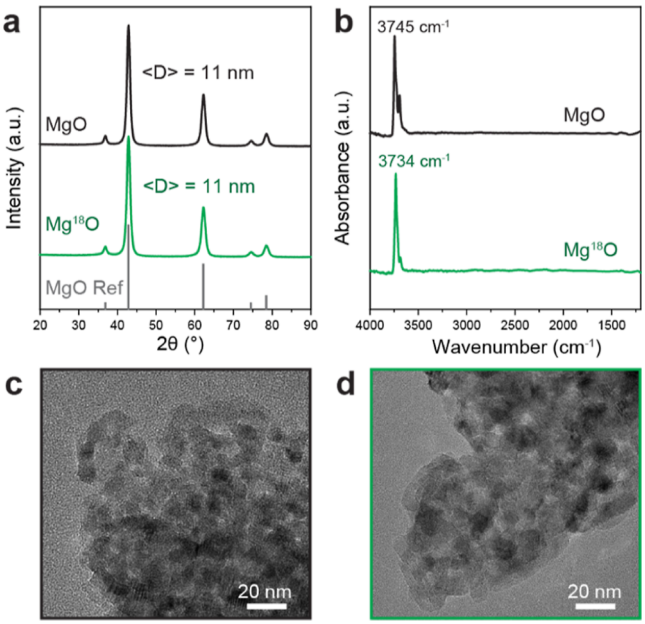

Figure 1. (a) Powder XRD patterns with the indication of the average crystallite size ($\langle D \rangle$), (b) FTIR spectra, and (c,d) TEM images of the as-synthesized unlabeled MgO and labeled $Mg^{18}O$ nanoparticles.

patterns, FTIR spectra, and TEM images of the as-synthesized MgO and ^{18}O-enriched MgO nanoparticles. Both the MgO and $Mg^{18}O$ nanoparticles are phase-pure and have a similar average crystallite size of 11 nm, as obtained by the Scherrer equation (Figure 1a). The nanocrystalline nature of both MgO and $Mg^{18}O$ is also clearly visible from the TEM images (Figure 1c), with the high surface area of, respectively, 121 and 126 m^2/g (Figure S1). Furthermore, the formation of clean, anhydrous MgO surfaces is demonstrated by IR spectroscopy by the absence of a broad band between 3200 and 3650 cm^{-1} (Figure 1b). The dehydrated nature of the as-prepared materials is important, as some of the carbonation experiments are performed in a closed system, and adsorbed water could induce exchange reactions with labeled ^{18}O.[38] Both MgO and $Mg^{18}O$ show sharp bands at ca. 3745 and 3734 cm^{-1}, respectively, which are due to isolated OH groups.[39,40] The isolated OH peak in $Mg^{18}O$ is blue-shifted (by 11 cm^{-1}) when compared to the peak in MgO, owing to the presence of the ^{18}O isotope. This shift matches well with the shift that would be expected in 100% ^{18}O-enriched MgO, indicating a very high enrichment level in the $Mg^{18}O$ sorbent prepared here.

Carbonation of $NaNO_3$-Promoted MgO with $C^{18}O_2$ to Disclose Intermediate Reaction Steps

We used $C^{18}O_2$ to probe the intermediate reaction steps in the carbonation reaction of $NaNO_3$-promoted MgO, that is, we aim to investigate to which extent the ^{18}O label of $C^{18}O_2$ is

https://doi.org/10.1021/jacsau.2c00461
JACS Au 2022, 2, 2731−2741

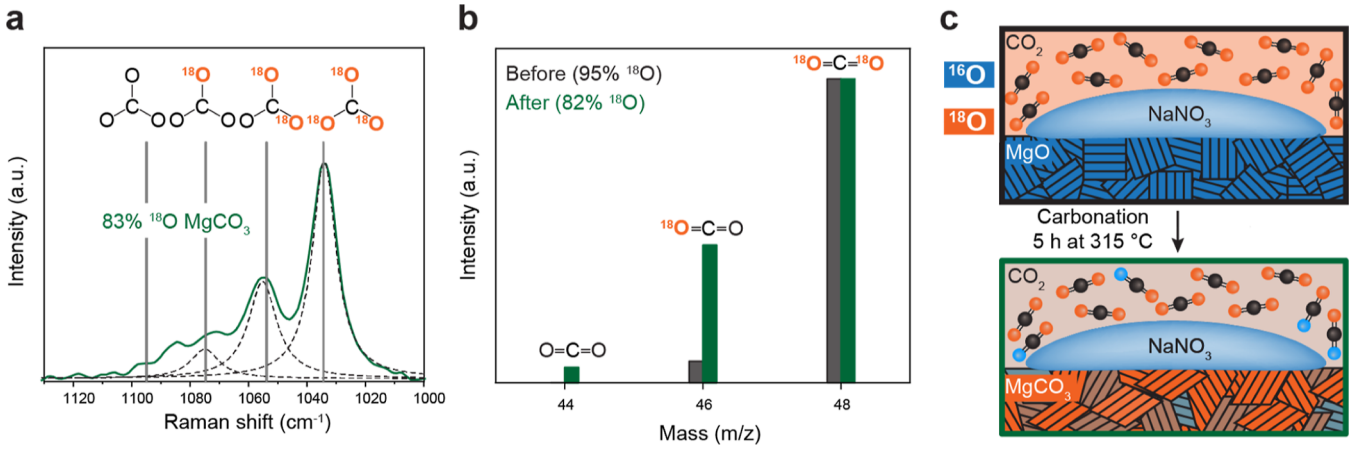

Figure 2. Carbonation of $NaNO_3$-promoted MgO using $C^{18}O_2$ in an autoclave at 300 °C for 5 h. (a) Raman spectrum of the carbonated material in the symmetric stretching region of $MgCO_3$. Peak positions for $MgCO_3$ containing 0, 1, 2, and 3 ^{18}O atoms are included (gray lines). Using Lorentzian functions' deconvolution (dashed lines) of the Raman spectrum, we deduce that after carbonation with $C^{18}O_2$, the magnesium carbonates formed contain mostly three ^{18}O atoms (with minor contributions of magnesium carbonates with 1 or 2 ^{18}O atoms). (b) Mass spectroscopy of the gas phase in the autoclave gives the distribution of ^{18}O in the gas-phase CO_2 before and after the carbonation experiment and reveals a reduction in the amount of ^{18}O in the gas phase after carbonation. (c) Schematic of a carbonation experiment in which $NaNO_3$-promoted MgO reacted with $C^{18}O_2$ in an autoclave. The location and quantity of ^{18}O label in the solid, molten, and gas phases before and after carbonation are highlighted by orange color. The figure illustrates that we observe ^{18}O label in $MgCO_3$ (orange color) but not in $NaNO_3$ (no color change) after the carbonation reaction.

incorporated into the product $MgCO_3$ and whether it is exchanged with the oxygen atoms of the $NaNO_3$ promoter. $NaNO_3$-promoted MgO was carbonated with $C^{18}O_2$ in an autoclave for 5 h at 300 °C and an initial $C^{18}O_2$ pressure of 1.3 bar (Figure 2). After 5 h, the $C^{18}O_2$ pressure was below 1 bar, and the conversion of MgO to $MgCO_3$ was 65%, as obtained via the Rietveld refinement of the XRD pattern acquired after carbonation (Figure S7 and Table S3).

The presence of ^{18}O in $MgCO_3$ and $NaNO_3$ was probed by Raman spectroscopy (Figure 2a). DFT simulations predict the symmetric stretching vibration of $MgCO_3$ in the Raman spectra to be shifted by 20 cm^{-1} to lower wavenumbers for each ^{18}O incorporated into the carbonate (Table S1). Hence, the peaks at 1094, 1074, 1054, and 1034 cm^{-1} in the Raman spectrum of ^{18}O-enriched $MgCO_3$ correspond to carbonates with 0, 1, 2, and 3 ^{18}O atoms, respectively (Figure 2a). Similarly, for $NaNO_3$, the symmetric stretching vibration at 1068 cm^{-1} in unlabeled $NaNO_3$ yields peaks at 1068, 1048, 1028, and 1008 cm^{-1} in ^{18}O-enriched $NaNO_3$, that is, corresponding to nitrate groups containing 0, 1, 2, and 3 ^{18}O atoms, respectively (Table S2). The ratio of the relative intensities of the carbonate (or nitrate) peaks expressed as peak areas is related to the relative quantities of $MgCO_3$ (or $NaNO_3$) containing 0, 1, 2, or 3 ^{18}O atoms. Unfortunately, the overlap of the bands due to ^{18}O-enriched $MgCO_3$ and ^{18}O-enriched $NaNO_3$ hinders their further quantification (Figure S2a). Therefore, we performed a washing step with deionized water at room temperature to separate $NaNO_3$ from $MgCO_3$ prior to Raman spectroscopy analysis (Figure S2). Peak fitting (using Lorentzian functions) of the Raman spectrum of $MgCO_3$ formed through the carbonation of $NaNO_3$-promoted MgO with $C^{18}O_2$ shows that the sample contains mostly $MgCO_3$ with three ^{18}O atoms and some minor quantities of $MgCO_3$ with one or two ^{18}O atoms. The total ^{18}O fraction in the carbonate is approximately 83% (see calculation in Figure S3). From eq 1, one would expect that the carbonation of unlabeled MgO with labeled $C^{18}O_2$ leads to an overall ^{18}O content of approximately 66% in the carbonate (i.e., two out of three oxygen atoms in $MgCO_3$ are ^{18}O). Therefore, to account for the additional ^{18}O label in the carbonate, there must be an oxygen exchange between either CO_2 and MgO or CO_2 and $MgCO_3$. The Raman spectrum of the recovered $NaNO_3$ part shows only one peak at 1068 cm^{-1}, corresponding to a nitrate that does not contain any ^{18}O label, indicating that there is no oxygen exchange between CO_2 and $NaNO_3$ (Figure S2b).

Furthermore, the analysis of the gas phase before and after carbonation in the autoclave by mass spectrometry (Figure 2b) shows a decrease in the ^{18}O content from an initial value of 95% ^{18}O to 82% ^{18}O after carbonation. This observation further evidences an oxygen exchange between CO_2 and MgO and/or between CO_2 and $MgCO_3$ during carbonation. Important to highlight is that the ^{18}O fraction in $MgCO_3$ is approximately equal to that in the remaining (unreacted) CO_2, indicative of an extensive scrambling of the oxygen atoms between the solid and gas phases over the 5 h carbonation experiment. In addition, this proves that there is no preferential incorporation of ^{16}O or ^{18}O in $MgCO_3$. Figure 2c gives a schematic of the system before and after carbonation, providing information on the location and quantity of ^{18}O in each phase.

To investigate whether the observed scrambling between the oxygen atoms in the solid sorbent and CO_2 is due to an oxygen exchange between crystalline $MgCO_3$ (i.e., involving lattice oxygens) and CO_2, the following experiment was performed. $NaNO_3$-promoted MgO after carbonation in an autoclave for 5 h with labeled $C^{18}O_2$ was exposed to unlabeled CO_2 for 5 h at 315 °C in a TG analyzer. After exposure to unlabeled CO_2, the ^{18}O fraction in $MgCO_3$ dropped only slightly from 83 to 80%, indicative of no scrambling between crystalline $MgCO_3$ and CO_2. If scrambling would have occurred, one would have expected the ^{18}O label in $MgCO_3$ to have reduced significantly. The slight drop in the ^{18}O fraction in $MgCO_3$ can be explained by the formation of new, unlabeled $MgCO_3$ upon the further carbonation of MgO with unlabeled CO_2. Indeed, the MgO conversion increased from 65 to 66% during the additional carbonation time with unlabeled CO_2 (Table S3) and a small

https://doi.org/10.1021/jacsau.2c00461
JACS Au 2022, 2, 2731−2741

peak at 1094 cm^{-1}, due to unlabeled $MgCO_3$, that appeared in the Raman spectrum (Figure S6). Overall, these results indicate that crystalline $MgCO_3$ does not exchange oxygen atoms with CO_2 under the employed carbonation conditions. Therefore, the observed scrambling reaction must have occurred between MgO and CO_2 (likely through the formation of surface carbonates).

Identifying the Reaction Stage during Carbonation at which the Oxygen Exchange Reaction between CO_2 and $NaNO_3$-Promoted $Mg^{18}O$ Occurs

To elucidate when (at which stage of the reaction) the oxygen exchange between CO_2 and MgO takes place, we employed *in situ* TGA–MS to probe the carbonation of $NaNO_3$-promoted $Mg^{18}O$ with unlabeled CO_2 (Figure 3). Such *in situ* TGA–MS experiments allow us to correlate the CO_2 uptake (TGA signal) with the evolution of ^{18}O-containing gaseous species (MS signal). Specifically, we probed whether the stream of CO_2 leaving the TGA instrument contains ^{18}O (MS signals at m/z = 46 for $C^{16}O^{18}O$ and m/z = 48 for $C^{18}O^{18}O$). Because of the high, constant flow of CO_2 (80 mL/min) over a sample of 50 mg of $NaNO_3$-promoted MgO, there is a background signal at m/z = 46 and m/z = 48 due to the natural abundance of ^{18}O (~0.2%). Therefore, the signals at m/z = 46 and m/z = 48 were corrected by subtracting the signal due to the natural abundance of ^{18}O (see Figure S8 for calculation) to monitor the ^{18}O released by the sorbent during the reaction.

The TGA uptake curve during the carbonation reaction of $NaNO_3$-promoted $Mg^{18}O$ (Figure S13) shows an induction period[41] (early stage of the carbonation reaction prior to the formation of bulk $MgCO_3$) of ca. 15 min featuring slow carbonation kinetics. The duration of the induction period can vary from less than 1 min up to 30 min depending on the sorbent synthesis method.[16,22,24,41,42] During the induction period, a large fraction of the ^{18}O label is released, yet no bulk $MgCO_3$ has formed. To obtain a clear trend between the CO_2 uptake and the release of ^{18}O label, a material with a short induction period is desirable. Therefore, $Mg^{18}O$ with a short induction period and fast kinetics ($Mg^{18}O_{(fast)}$) was prepared from the as-synthesized, slowly carbonating $Mg^{18}O$ ($Mg^{18}O_{(slow)}$) (see more details in ESI, Figure S11).

The weight increase and the derivative of the weight increase during the first 15 min of the carbonation of $NaNO_3$-promoted $Mg^{18}O_{(fast)}$ at 315 °C with unlabeled CO_2 (Figure 3a) show three distinct reaction stages: (i) rapid formation of surface carbonates, (ii) bulk carbonation described by the Avrami–Erofeev model, and (iii) slow, diffusion-controlled carbonation, with the carbonation rate asymptotically approaching zero, as described in the literature through kinetic modeling.[16,43] After 2 h of carbonation, the conversion was 41% (as calculated from the TGA data and confirmed by Rietveld refinement of the XRD pattern of the carbonated material, see Figure S12). The three reaction stages, as identified in the TGA signal, are also clearly visible in the MS signals at m/z = 46 and m/z = 48 (Figure 3b). In the first stage, there is a spike in the signals at m/z = 46 and m/z = 48, indicating that an oxygen exchange reaction takes place during the surface carbonation stage. In the second reaction stage, the signals for ^{18}O-labeled CO_2 follow the same trend as the derivative of the weight change, that is, the faster the rate of carbonation, the more ^{18}O is exchanged and released in the form of ^{18}O-labeled CO_2. In the third stage of the carbonation reaction, the signals at m/z = 46 and m/z = 48 drop and asymptotically approach zero,

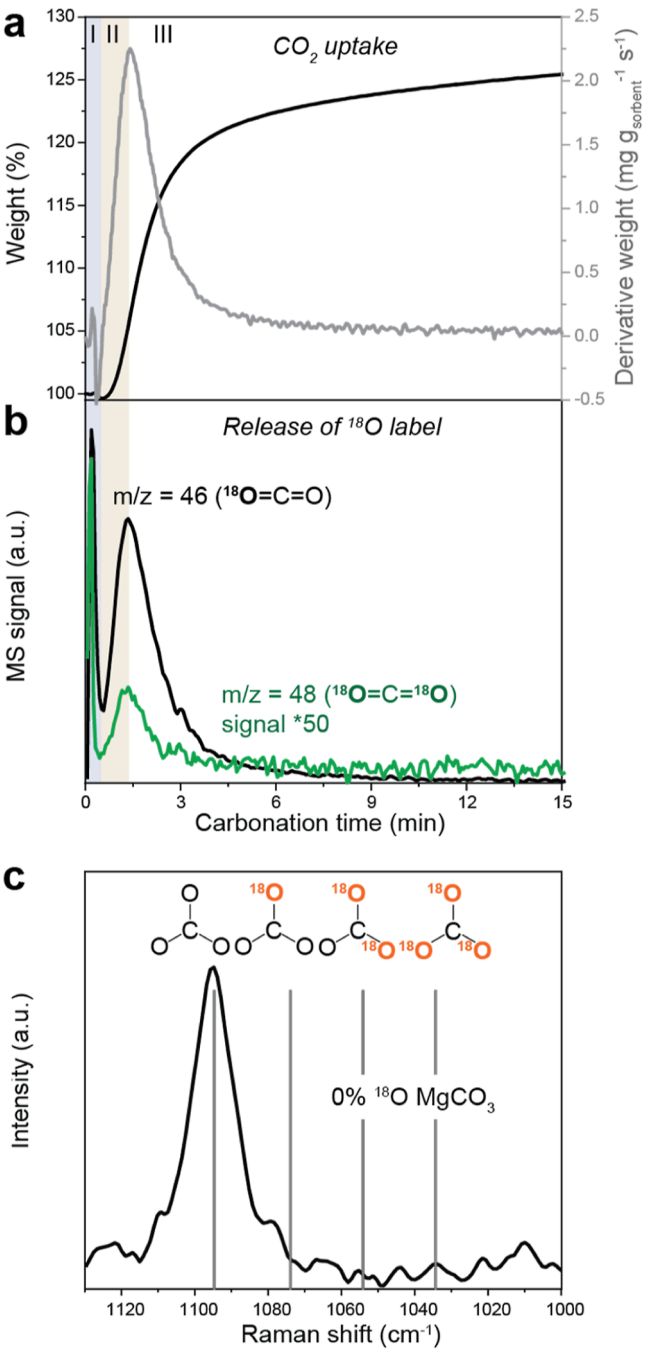

Figure 3. *In situ* TGA–MS experiments probing the release of ^{18}O-containing CO_2 in the gas phase during the carbonation of $NaNO_3$-promoted $Mg^{18}O_{(fast)}$ with unlabeled CO_2 at 315 °C (flow experiment). Three different reaction stages labeled I, II, and III are identified. (a) TGA data showing the weight increase (where 100% represents the sorbent weight at the beginning of the carbonation) and the derivative of the weight increase. (b) Natural abundance-corrected MS signals at m/z = 46 and m/z = 48 as a function of time. An excellent kinetic agreement is found between the rate of weight increase (~carbonation rate) and the release of ^{18}O-labeled CO_2. (c) Raman spectrum of $NaNO_3$-promoted $Mg^{18}O$ after carbonation for 2 h in the TGA instrument with unlabeled CO_2 in the symmetric stretching region of $MgCO_3$. Peak positions for $MgCO_3$ with 0, 1, 2, and 3 ^{18}O atoms are included (gray lines). The formed $MgCO_3$ contains only one peak, that is, corresponding to $MgCO_3$ with no ^{18}O atoms.

https://doi.org/10.1021/jacsau.2c00461
JACS Au 2022, 2, 2731–2741

following again the same trend as observed for the carbonation rate. These TGA−MS results reveal that the oxygen exchange between CO_2 and MgO took place in the very first stage of the carbonation reaction. Indeed, the oxygen exchange reaction occurs both during the initial surface carbonation and the formation of bulk $MgCO_3$. Once the carbonation reaction has finished, no further oxygen exchange reaction occurs. Note that after the initial weight gain in stage I, there is a small drop in the sample weight. This is due to the replacement of heavy ^{18}O with lighter ^{16}O in MgO (vide infra).

Further insight into the oxygen exchange process is obtained through the Raman analysis of the material after the TGA−MS experiment (Figure 3c). The Raman spectrum shows only one peak at 1094 cm^{-1} corresponding to unlabeled $MgCO_3$, although the $NaNO_3$-promoted $Mg^{18}O_{(fast)}$ had a high ^{18}O fraction at the start of the carbonation reaction (Figure S11). This observation demonstrates that the oxygen exchange reaction is very fast, leading to the complete exchange of all ^{18}O atoms in MgO with ^{16}O atoms from CO_2 prior to $MgCO_3$ crystal formation (flow system experiment). Note that the carbonation of $NaNO_3$-promoted $Mg^{18}O$ with unlabeled CO_2 in an autoclave (closed system experiment) leads to $MgCO_3$ with 16% ^{18}O because the exchanged, labeled CO_2 cannot leave the reactor and can therefore be incorporated into the formed $MgCO_3$ (Figure S4). The ^{18}O fraction in the remaining (unreacted) CO_2 is 14%, which is very similar to the ^{18}O fraction in $MgCO_3$.

Role of $NaNO_3$ in the Dynamic Formation and Dissolution of Surface Carbonates

Next, we probe the role of $NaNO_3$ in the oxygen exchange reaction between CO_2 and MgO. To this end, we compare the oxygen exchange behavior of unpromoted $Mg^{18}O_{(slow)}$ with that of $NaNO_3$-promoted $Mg^{18}O_{(slow)}$ during carbonation. For this study, we use a sample with a long induction period as we are interested in the early stages of the carbonation reaction that is prior to the formation of bulk $MgCO_3$ in $NaNO_3$-promoted MgO (i.e., ca. the first 15 min, as also confirmed by XRD, Figure S15). Indeed, a comparison between unpromoted and $NaNO_3$-promoted MgO is only meaningful in the induction period, as in the absence of $NaNO_3$, the exposure of MgO to a CO_2 atmosphere solely leads to the formation of surface carbonates (i.e., without the formation of bulk $MgCO_3$).[20]

Figure 4 plots the TGA−MS results of unpromoted and $NaNO_3$-promoted $Mg^{18}O_{(slow)}$ during the first 12 min of carbonation with unlabeled CO_2. Both materials show a very rapid, initial weight increase (Figure 4a), which is due to the formation of surface carbonates, as confirmed by FTIR analysis (Figure S16). During this period of rapid CO_2 uptake, there is a spike in the signal for ^{18}O-labeled CO_2 (m/z = 46 and m/z = 48) (Figure 4b), providing strong evidence that the oxygen exchange occurs during the formation of surface carbonates. After the initial weight gain (t > 1 min), unpromoted $Mg^{18}O_{(slow)}$ only shows a slight increase in its sample weight, and after 12 min of carbonation, the sample weight stabilized. In contrast, after the initial, rapid weight increase, $NaNO_3$-promoted $Mg^{18}O_{(slow)}$ shows a drop in the sample weight. A reference experiment using $NaNO_3$-promoted, but unlabeled, MgO does not show this decrease in sample weight (Figure S13), indicating that the loss in sample weight for t > 1 min is related to a loss (i.e. exchange) of ^{18}O that is replaced by ^{16}O. Furthermore, the inset in Figure 4b shows that when using

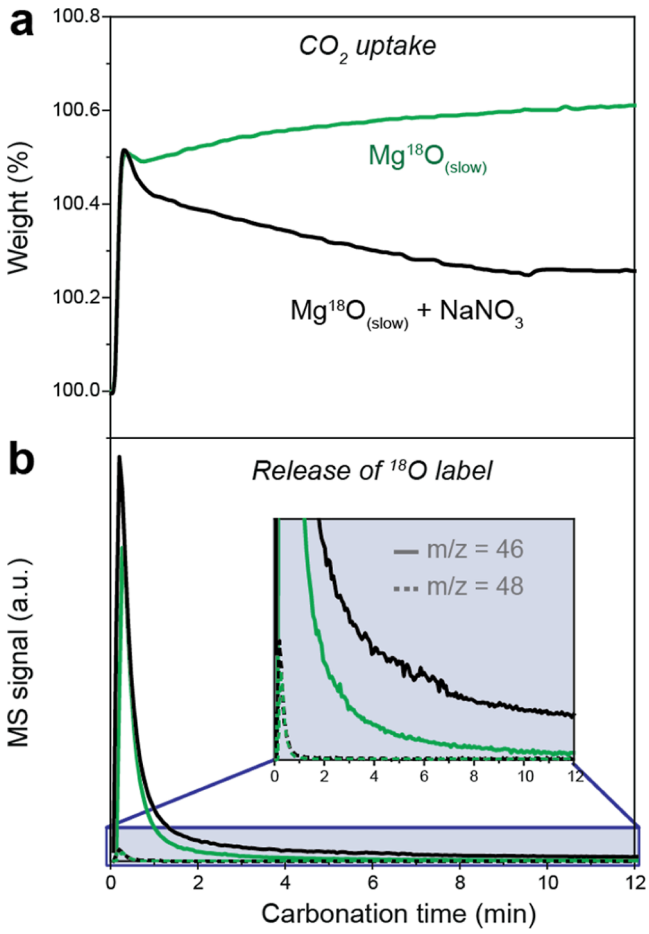

Figure 4. Oxygen exchange reaction between $Mg^{18}O_{(slow)}$ and CO_2 during the first 12 min of the carbonation reaction at 315 °C: comparing the behavior of unpromoted (green) and $NaNO_3$-promoted $Mg^{18}O_{(slow)}$ (black). Both the acquired TGA data (where 100% represents the sorbent weight at the beginning of the carbonation) (a) and MS data showing the signals at m/z = 46 (full lines) and m/z = 48 (dashed lines) (b) reveal a very similar behavior of unpromoted and $NaNO_3$-promoted $Mg^{18}O_{(slow)}$ at the very beginning of the carbonation reaction (i.e., t < 1 min), that is, evidencing that fast oxygen exchange reactions occur in both materials. The inset in b shows that the signal at m/z = 46 drops to zero after 12 min of carbonation for unpromoted $Mg^{18}O_{(slow)}$, while it does not approach zero for $NaNO_3$-promoted $Mg^{18}O_{(slow)}$.

unpromoted $Mg^{18}O_{(slow)}$, the signal at m/z = 46 drops to zero after 12 min, while for $NaNO_3$-promoted $Mg^{18}O_{(slow)}$, the signal is considerably higher during the entire duration of the carbonation reaction and does not approach zero within the time considered.

We can explain the simultaneous weight increase (TGA) and loss of ^{18}O in the form of $C^{18}O^{16}O$ and $C^{18}O_2$ (MS) at the beginning of the carbonation reaction by a surface carbonate-mediated oxygen exchange mechanism. Indeed, Tsuji et al. and others have provided some evidence for an oxygen exchange reaction to occur between MgO and $C^{18}O_2$.[44,45] In their study, $C^{18}O_2$ was first adsorbed on MgO at room temperature, and subsequently the isotopic composition of the desorbed CO_2 was measured during temperature-programmed desorption. It was observed that both single and double oxygen exchanges took place. The single oxygen exchange reaction takes place through a bidentate carbonate intermediate and the double oxygen exchange by sequential binding and unbinding of CO_2

https://doi.org/10.1021/jacsau.2c00461
JACS Au 2022, 2, 2731−2741

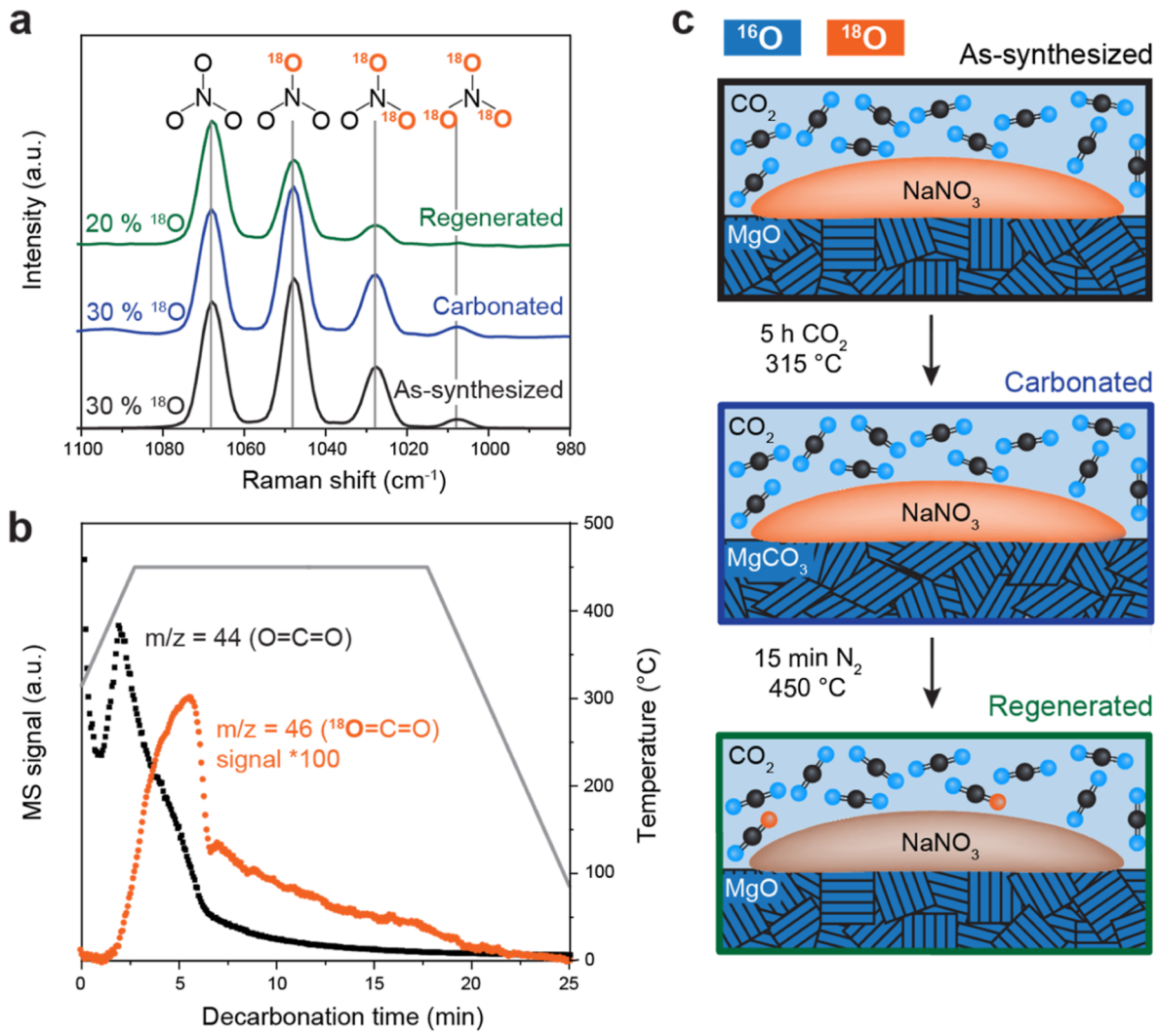

Figure 5. (a) Raman spectra in the $NaN^{18}O_3$ region of the as-synthesized, carbonated, and regenerated samples. Peak positions for $NaNO_3$ with 0, 1, 2, and 3 ^{18}O atoms are included (gray lines). (b) MS signal at m/z = 44 and m/z = 46 during the regeneration of $NaN^{18}O_3$-promoted $MgCO_3$ ($NaN^{18}O_3$-promoted MgO after 5 h of carbonation with CO_2 at 315 °C) at 450 °C in N_2. (c) Schematic representation of $NaN^{18}O_3$-promoted MgO in its as-synthesized, carbonated, and regenerated (calcined) states. The location and quantities of the ^{18}O label are indicated by orange color in each phase. During carbonation, the ^{18}O label remains in $NaNO_3$, while during regeneration, a part of the ^{18}O label is exchanged with the CO_2 atmosphere (loss of ^{18}O in $NaNO_3$ is illustrated by the faded orange color).

through the migration of the bidentate carbonate on the MgO surface. Translated to our high-temperature system, this implies that CO_2 adsorption on MgO at 315 °C and 1 bar CO_2 is not a static process but instead highly dynamic. CO_2 rapidly adsorbs and desorbs and can even migrate on the MgO surface. Note that this is different from what is generally reported in the literature, that is, that surface carbonates on MgO form a rigid, CO_2-impermeable layer.[24,37]

The oxygen exchange reaction was observed both for unpromoted and promoted $Mg^{18}O_{(slow)}$, indicating that the oxygen exchange reaction is not inherently linked to the presence of a promoter. Nevertheless, we observe a difference in the extent of the oxygen exchange reaction between unpromoted and promoted $Mg^{18}O_{(slow)}$. In the case of unpromoted $Mg^{18}O_{(slow)}$, there is no MS signal at m/z = 46 after 12 min of carbonation, most likely because all surface ^{18}O has been exchanged. In contrast, for $NaNO_3$-promoted $Mg^{18}O_{(slow)}$ the oxygen exchange reaction continues during the entire 12 min of carbonation and also shows a drop in sample weight. The drop in sample weight is explained by the partial substitution of the heavier ^{18}O with lighter ^{16}O in $Mg^{18}O$ through a surface bidentate carbonate. Thus, $^{18}O-^{16}O$ exchange via surface carbonates occurs to a higher extent (evidenced by a larger area under the curve which extends over longer times) in promoted $Mg^{18}O$. Possible explanations for the higher degree of oxygen exchange for promoted $Mg^{18}O$ include an enhanced mobility of oxygen on the MgO surface in the presence of $NaNO_3$ and/or the generation of additional surface $Mg^{18}O$ through the formation of dissolution pits, leading to an increased surface area. Surface dissolution of MgO in the presence of $NaNO_3$ has been reported previously and is manifested in the formation of etching pits which provide additional MgO surface area.[27]

The TGA–MS data for the entire duration of the carbonation reaction (i.e., up to t = 2 h) of $NaNO_3$-promoted $Mg^{18}O_{(slow)}$ show that bulk $MgCO_3$ starts to form after 15 min, as evidenced from an increase in the sample weight (Figure S13). During bulk $MgCO_3$ formation, there is an increase in the MS signal at m/z = 46. This agrees with the results shown in Figure 3, in that the intensity of the m/z = 46 signal is

https://doi.org/10.1021/jacsau.2c00461
JACS Au 2022, 2, 2731–2741

proportional to the carbonation rate. The formation of $MgCO_3$ leads to the formation of new exposed $Mg^{18}O$ surfaces, upon dissolution of $[Mg^{2+}\cdots O^{2-}]$ or $[Mg^{2+}\cdots CO_3^{2-}]$ ion pairs in the melt (vide infra), followed by $MgCO_3$ crystallization at a nucleation point. The newly exposed $Mg^{18}O$ surface readily exchanges oxygen atoms through adsorbing and desorbing CO_2 prior to its conversion to $MgCO_3$. Hence, the ^{18}O labeling experiments give a strong indication that $MgCO_3$ formation takes place via a dissolution−crystallization mechanism. This is in agreement with the work of Bork et al. in that they observed etching pits on the surface of a carbonated MgO single crystal in the proximity of $MgCO_3$.[27] Here, our results show that the formation of surface carbonates precedes the dissolution step and suggest that surface carbonates dissolve in the nitrate melt as $[Mg^{2+}\cdots CO_3^{2-}]$ ion pairs.

Do Oxygen Atoms from $NaNO_3$ Participate in the Carbonation Reaction?

It has been suggested that the decomposition products of molten alkali metal nitrates, specifically O^{2-}, NO_2^-, and NO_2^+, might play a role in the promotion mechanism of MgO-based CO_2 sorbents.[24,37,46] In molten alkali metal nitrates, the nitrate ion can self-dissociate according to

$$NO_3^- \rightleftharpoons NO_2^+ + O^{2-} \quad (2)$$

Kust et al. determined potentiometrically that the oxygen ion concentration at 300 °C formed by eq 2 is 2×10^{-7} mol L^{-1}, corresponding to 8×10^{-11} mol g_{MgO}^{-1} for a typical $NaNO_3$-promoted MgO sorbent, which is 8 orders of magnitude lower than the oxygen concentration at the surface of MgO (see Figure S17 for calculations).[47,48] Furthermore, alkali metal nitrates heated to temperatures above their melting point can thermally decompose, leading to the formation of nitrites[49]

$$NO_3^- \rightleftharpoons NO_2^- + 1/2O_2 \quad (3)$$

At 315 °C, the decomposition of the nitrate ion is limited, and the concentration of the decomposition products is very low.[50,51] Yet, little is known about the effect of MgO and CO_2 on the equilibria of these reactions. One possibility is that the CO_2 atmosphere (during carbonation) affects the equilibria of eqs 2 and (3). For example, CO_2 dissolved in the molten alkali metal nitrates could react with O^{2-} to form CO_3^{2-}, which would drive the equilibrium of reaction 2 to the right-hand side. If the decomposition products of the nitrate ion actively participate in the carbonation reaction, the oxygen atoms of the nitrate ion would be incorporated into the formed $MgCO_3$. To investigate this hypothesis, we performed ^{18}O-labeling experiments using MgO promoted with ^{18}O-labeled $NaNO_3$. $NaN^{18}O_3$-promoted MgO was carbonated for 5 h at 315 °C in CO_2, followed by regeneration at 450 °C in N_2 for 15 min in a TGA system (Figure S19). The as-synthesized ^{18}O-enriched $NaNO_3$ had a high phase purity, as demonstrated by XRD (Figure S18). Figure 5a shows the Raman spectra of the $NaN^{18}O_3$ part of the as-synthesized, carbonated, and regenerated $NaN^{18}O_3$-promoted MgO. After 5 h of carbonation, there is no change in the ^{18}O fraction in $NaN^{18}O_3$. This indicates that the oxygens of $NaNO_3$ do not actively participate in the carbonation reaction. However, after the regeneration step (treatment in N_2 at 450°C in which $MgCO_3$ decomposes back to MgO), the ^{18}O fraction in the nitrate reduced from 30 to 20%. The TGA−MS data acquired during the regeneration of carbonated $NaN^{18}O_3$-promoted MgO at 450 °C in N_2 reveal the origin of the loss of ^{18}O label during the sorbent regeneration step (Figure 5b). When heating in N_2, we observe an increase in the MS signal at $m/z = 44$ ($C^{16}O_2$) for $T > 365$ °C due to the decomposition of $MgCO_3$. For $T > 390$ °C, the signal at $m/z = 46$ ($C^{18}O^{16}O$) also starts to appear. After 5 min at 450 °C, both the signals at $m/z = 44$ and $m/z = 46$ slowly disappear as most of the$MgCO_3$ has been decomposed. The ^{18}O label in the released CO_2 does not originate from $MgCO_3$ because no ^{18}O label was detected in $MgCO_3$ formed after 5 h of carbonation (Figure S21), and the signal for $C^{18}O^{16}O$ appears at a higher temperature than the signal for $C^{16}O_2$ (however $C^{16}O_2$ and $C^{18}O^{16}O$ desorb at exactly the same temperature from ^{18}O-labeled $MgCO_3$, see Figure S22). Therefore, the MS signal at $m/z = 46$ ($C^{18}O^{16}O$) at temperatures >390 °C must originate from an oxygen exchange between ^{18}O-labeled $NaNO_3$ and CO_2 (or between ^{18}O-labeled $NaNO_3$ and $MgCO_3$). In addition, when the regeneration was performed at a lower temperature of 370 °C, there was no loss of ^{18}O label (Figures S19 and S20), indicating that the oxygen exchange between $NaNO_3$ and CO_2 during sorbent regeneration is temperature-dependent. Figure 5c sketches the location and quantity of ^{18}O in the different phases of the system for the as-synthesized, carbonated, and regenerated material. Due to the absence of any oxygen exchange involving $NaNO_3$ during the carbonation reaction, we can conclude that at the operating temperature of the carbonation reaction (315 °C) the nitrate group of $NaNO_3$ does not actively participate in the carbonation reaction and that the small concentrations of O^{2-} in molten nitrates do very likely not play a crucial role in the promotion of the carbonation reaction. It is more likely that molten $NaNO_3$ acts as a "solvent" that promotes the carbonation reaction through the accelerated dissolution of $[Mg^{2+}\cdots CO_3^{2-}]$ ion pairs.

Carbonation Mechanism

Recently, Gao et al. have proposed a reaction mechanism in which the promotional effect of $NaNO_3$ is described through the decomposition of NO_3^- into NO_2^+ and O^{2-}, based on the results of transient ^{18}O-isotopic exchange experiments.[37] NO_2^+ promotes the carbonation reaction by adsorbing on MgO, which lowers the energy barrier of $[Mg^{2+}\cdots O^{2-}]$ ion pair dissolution into $NaNO_3$, as evidenced from their DFT calculations. However, our ^{18}O labeling experiments clearly show that the decomposition products of $NaNO_3$ do not actively participate in the carbonation reaction. Therefore, we have excluded that possibility in our DFT calculations.

Our experimental observations point toward a mechanism in which the molten salt acts as a solvent. Therefore, we have assessed the energetics of two possible pathways, involving either the dissolution of $[Mg^{2+}\cdots O^{2-}]$ ion pairs or $[Mg^{2+}\cdots CO_3^{2-}]$ ion pairs in $NaNO_3$ using AIMD calculations (Figure 6). Our calculations show that the dissolution energy for an $[Mg^{2+}\cdots O^{2-}]$ ion pair in $NaNO_3$ is 3.56 eV, which is appreciably higher than that for an $[Mg^{2+}\cdots CO_3^{2-}]$ ion pair (1.1 eV). Further, we find that it is energetically favorable for a CO_2 molecule to bind to the MgO(001) surface (−0.54 eV). Based on these computations, we hypothesize that CO_2 molecules first interact with MgO, leading to the formation of surface carbonates, which eventually dissolve into the $NaNO_3$ melt forming $[Mg^{2+}\cdots CO_3^{2-}]$ ion pairs and subsequently crystallize to bulk $MgCO_3$. Furthermore, the surface carbonate-intermediated oxygen exchange between MgO and

https://doi.org/10.1021/jacsau.2c00461
JACS Au 2022, 2, 2731−2741

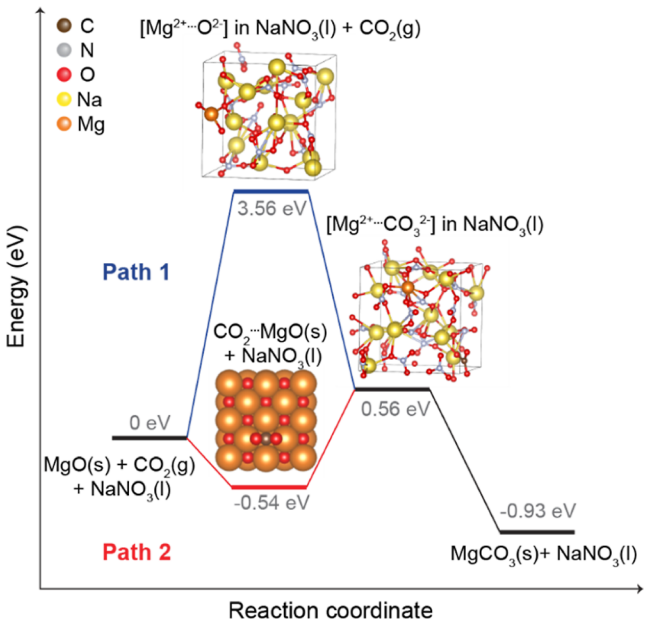

Figure 6. Possible reaction pathways for the carbonation reaction of $NaNO_3$-promoted MgO involving either the dissolution of $[Mg^{2+}\cdots O^{2-}]$ ion pairs (path 1) or $[Mg^{2+}\cdots CO_3^{2-}]$ ion pairs (path 2). Pathway 2 is energetically more favorable and in line with our experimental observations. The insets show the structural models used for the DFT and AIMD calculations of adsorbed CO_2 on the MgO(100) surface, the $[Mg^{2+}\cdots O^{2-}]$ ion pair in molten $NaNO_3$, and the $[Mg^{2+}\cdots CO_3^{2-}]$ ion pair in molten $NaNO_3$.

CO_2 prior to bulk $MgCO_3$ formation can be explained by the low energy barrier for an adsorbed CO_2 molecule to desorb again from the MgO surface (0.54 eV) as compared to the energy barrier for the dissolution of surface carbonates as $[Mg^{2+}\cdots CO_3^{2-}]$ ion pairs into $NaNO_3$ (1.1 eV), which is the rate-limiting step in the carbonation mechanism.

CONCLUSIONS

A series of ^{18}O labeling experiments on model MgO-based CO_2 sorbents, performed under well-controlled conditions and using a combination of Raman spectroscopy, TGA–MS, and atomistic modeling, allowed us to elucidate important aspects of the complex carbonation mechanism of $NaNO_3$-promoted MgO. Carbonation experiments performed in an autoclave show that there is a complete scrambling of oxygen atoms between CO_2 and surface carbonates, while bulk $MgCO_3$ does not exchange oxygen atoms with CO_2. In addition, from the *in situ* TGA–MS analysis during the carbonation of $NaNO_3$-promoted $Mg^{18}O$, we could follow the degree of the oxygen exchange reaction between MgO and CO_2 with time. We find that the rate of the oxygen exchange reaction is proportional to the rate of CO_2 uptake and ultimately leads to the complete loss of ^{18}O, indicating that oxygen exchange is a very rapid process. The oxygen exchange reaction proceeds through the reversible formation and decomposition of surface carbonates, both in the presence and absence of $NaNO_3$. Moreover, the presence of $NaNO_3$ enhances the oxygen exchange, very likely due to the continuous generation of fresh MgO surfaces through a $NaNO_3$-promoted etching mechanism. These results reveal the highly dynamic nature of surface carbonates under CO_2 capture conditions. Importantly, during the carbonation reaction, we could not detect any oxygen exchange reaction involving the oxygen atoms of $NaNO_3$. Combining these experimental findings with DFT and AIMD modeling, we postulate that the carbonation mechanism of $NaNO_3$-promoted MgO involves the rapid formation of surface carbonates, followed by their dissolution, yielding $[Mg^{2+}\cdots CO_3^{2-}]$ ion pairs in the $NaNO_3$ melt and the crystallization of $MgCO_3$ at the MgO–$NaNO_3$ interface. The insight on the carbonation mechanism obtained in this work will guide the designing of more effective MgO-based CO_2 sorbents by having identified the solubility of $[Mg^{2+}\cdots CO_3^{2-}]$ ion pairs in the molten salt promoter as a key parameter for high activity. In addition, we believe that the methods described in this work are highly versatile and can be applied to investigate the reaction mechanisms of different families of solid oxide CO_2 sorbents and thereby advance their development.

EXPERIMENTAL SECTION

Materials

Magnesium nitride (Mg_3N_2, 99.5%), ^{18}O-labeled water ($H_2{}^{18}O$, 97 atom % ^{18}O), nitric acid (HNO_3, 70%, ACS reagent), sodium nitrate ($NaNO_3$, 99.995%, anhydrous), and ^{18}O-labeled carbon dioxide ($C^{18}O_2$, 95 atom % ^{18}O) were purchased from Sigma-Aldrich. Sodium carbonate (Na_2CO_3, 99.5%) was purchased from Acros Organics.

Material Synthesis

^{18}O-enriched $Mg(OH)_2$ was synthesized by reacting 0.5 g Mg_3N_2 with 0.55 mL of 97% ^{18}O-enriched water. ^{18}O-enriched MgO was prepared by heat treatment of ^{18}O-enriched $Mg(OH)_2$ under high vacuum ($<10^{-5}$ mbar) at 700 °C (heating rate of 10 °C min^{-1}) for 6 h. ^{18}O-enriched MgO was stored under an inert atmosphere to prevent any loss of ^{18}O by exchange with H_2O and O_2 in air. The unlabeled MgO material was prepared in an identical fashion, replacing ^{18}O-enriched water by conventional deionized water.

^{18}O-enriched $NaNO_3$ was synthesized according to a previously described method.[52] Briefly, 100 μL of 70% HNO_3 was equilibrated with 140 μL of 97% ^{18}O-enriched water for 3 days at 100 °C in a closed vial. Afterward, the solution was neutralized with 82.4 mg Na_2CO_3. Subsequently, water was evaporated via heating to 100 °C at a pressure of 1 mbar for 24 h, yielding ^{18}O-enriched $NaNO_3$ with an ^{18}O fraction of 30%.

$NaNO_3$-promoted MgO was prepared by grinding MgO (or $Mg^{18}O$) with anhydrous $NaNO_3$ (or the synthesized ^{18}O-enriched $NaNO_3$) (Na/Mg molar ratio of 1:10) with a mortar and pestle under a N_2 atmosphere. The $NaNO_3$-promoted $Mg^{18}O$ prepared in this way is referred to as $NaNO_3$-promoted $Mg^{18}O_{(slow)}$. The preparation of $NaNO_3$-promoted $Mg^{18}O_{(fast)}$ from $NaNO_3$-promoted $Mg^{18}O_{(slow)}$ is described in the Supporting Information (Figure S11).

Characterization

XRD data were collected using a PANalytical Empyrean X-ray powder diffractometer equipped with a Bragg–Brentano HD mirror and operated at 45 kV and 40 mA using Cu Kα radiation. The scans were collected in the 2θ range of 15–90° (step size, 0.033° and time per step, 3.2 s). Raman spectra were collected with a Thermo Scientific DXR2 Raman spectrometer equipped with a 532 nm laser using a spot size of 1.8 μm. The spectra were acquired in the range of 100–3,500 cm^{-1} with a spectral resolution of 0.964 cm^{-1}. Five measurements at different locations of the sample with a measurement time of 100 s were acquired and averaged. FTIR spectroscopy experiments were performed on self-supporting pellets using a Bruker Alpha II spectrometer in transmission mode (12 scans, 2 cm^{-1} resolution) under a N_2 atmosphere. TEM measurements were acquired with a FEI Talos F200X electron microscope operated at 200 kV. BET (Brunauer–Emmett–Teller) surface areas of the materials were measured from the N_2 physisorption isotherms recorded at 77 K on an Anton Paar Nova 800 apparatus. The samples were degassed at 300 °C under vacuum (10–3 mbar) for 3 h prior to measurement.

https://doi.org/10.1021/jacsau.2c00461
JACS Au 2022, 2, 2731–2741

Batch Carbonation Inside an Autoclave

An amount of 80 mg of the sorbent was loaded into an alumina crucible and placed into a 100 mL autoclave (Figure S23). The sample loading was performed in N_2 to prevent any adsorption of water or CO_2 by the sorbent. Then, the N_2-filled autoclave was heated to 300 °C on a hotplate. At 300 °C, the autoclave was evacuated to a pressure of 5 mbar for 5 min. Subsequently, the autoclave was filled with CO_2 or ^{18}O-enriched CO_2 (Sigma-Aldrich, 95% enrichment) to a pressure of 1.3 bar. The autoclave was kept at 300 °C for 5 h for the carbonation reaction to take place. During the reaction, the pressure gradually dropped to a pressure below 1 bar. Afterward, the autoclave was cooled down to room temperature and pressurized to 3.5 bar with N_2. Finally, the outlet of the autoclave was connected to a mass spectrometer to analyze the isotopic composition of the remaining CO_2. The signals for the following masses (m/z) were acquired: 28 (N_2), 44 (CO_2), 46 ($CO^{18}O_2$), and 48 ($C^{18}O_2$).

TGA–MS Experiments

TGA experiments were carried out on a Mettler Toledo TGA/DSC 3+ instrument. In a typical analysis, 50 mg (10 mg for the experiment in Figure 3) of the sample powder was loaded into an alumina crucible. The flow of reactive gas (N_2 for pretreatment and regeneration and CO_2 for carbonation) passing over the sample was set to 80 mL min^{-1}, and a heating rate of 50 °C min^{-1} was used unless stated otherwise. During the entire experiment, the gas phase was analyzed by a mass spectrometer (MKS Cirrus TM 3-XD). The signals for the following masses (m/z) were acquired: 18 (H_2O), 20 ($H_2{}^{18}O$), 28 (N_2), 30 (NO), 32 (O_2 or $N^{18}O$), 44 (CO_2), 46 ($CO^{18}O_2$, NO_2), and 48 ($C^{18}O_2$). More details on the TGA–MS experiments, including the alignment of the TGA and MS data in time, effects of mass-transfer resistance, and the reproducibility of the TGA–MS experiments, are given in the Supporting Information (Figures S24 and S25).

Computational Methods

All DFT calculations and AIMD simulations were performed using a plane-wave basis set, as implemented in VASP.[53,54] The projector augmented-wave method was used to describe the core electrons[55] with the Perdew–Burke–Ernzerhof exchange–correlation (XC) functional.[56] The kinetic energy cutoff for the wave function and charge density was set to 500 eV, and converged k-grids were used. DFT relaxations proceeded until the residual forces were less than 0.03 eV/Å.

Raman spectra calculations were also carried out using VASP, following the procedure given by Liang and Meunier.[57]

CO_2 Adsorption on MgO. To calculate the adsorption energy of CO_2 on a MgO(100) surface, we modeled the MgO(100) surface using the slab method. The structures consisted of four MgO layers. To model the surface–bulk interactions, only the uppermost two layers of MgO(100) were allowed to relax, while the rest of the atoms were fixed in their bulk coordinates.

MgO and $MgCO_3$ Dissolution in $NaNO_3$. We computed the total energy values of the molten $NaNO_3$ matrix (E_{NaNO_3}) and the same with [$Mg^{2+}\cdots O^{2-}$] or [$Mg^{2+}\cdots CO_3{}^{2-}$] ion pairs ($E_{ionpair/NaNO_3}$) using AIMD simulations. To compute E_{NaNO_3}, we placed 13 [$Na^+\cdots NO_3{}^-$] units randomly in a unit cell measuring 10 Å × 10 Å× 10 Å using the Packmol code.[58] Two MD runs were carried out on this structure using the *NVT* ensemble and a Nose–Hoover thermostat. In the first run, we heated the system from 300 to 600 K over 5 ps. In the second run, we annealed the system at 600 K for 5 ps. We computed the total energy by taking the average of the final 2 ps. This is the total energy obtained for one configuration. We ran three such configurations, and the final total energy, E_{NaNO_3}, is obtained as the average for the three configurations to obtain a statistically meaningful value. To compute $E_{ionpair/NaNO_3}$, we followed the same methodology as given above for E_{NaNO_3}, the only difference being that we inserted one ion pair randomly in the $NaNO_3$ structure created above.

ASSOCIATED CONTENT

Supporting Information

The Supporting Information is available free of charge at https://pubs.acs.org/doi/10.1021/jacsau.2c00461.

Additional description of methods, autoclave carbonation setup, DFT-calculated Raman shifts of ^{18}O-labeled materials, calculation of ^{18}O fraction in $MgCO_3$ and $NaNO_3$, Rietveld refinement of XRD data, FTIR data of surface carbonates on MgO, and supplementary results including TGA, MS, Raman, N_2 physisorption, and XRD data (PDF)

AUTHOR INFORMATION

Corresponding Author

Christoph R. Müller − *Laboratory of Energy Science and Engineering, Department of Mechanical and Process Engineering, Eidgenössische Technische Hochschule (ETH) Zürich, Zürich 8092, Switzerland;* orcid.org/0000-0003-2234-6902; Email: muelchri@ethz.ch

Authors

Annelies Landuyt − *Laboratory of Energy Science and Engineering, Department of Mechanical and Process Engineering, Eidgenössische Technische Hochschule (ETH) Zürich, Zürich 8092, Switzerland;* orcid.org/0000-0003-4045-5360

Priyank V. Kumar − *School of Chemical Engineering, The University of New South Wales (UNSW Sydney), Sydney, New South Wales 2052, Australia;* orcid.org/0000-0002-8203-7223

Jodie A. Yuwono − *School of Chemical Engineering, The University of New South Wales (UNSW Sydney), Sydney, New South Wales 2052, Australia;* orcid.org/0000-0002-0915-0756

Alexander H. Bork − *Laboratory of Energy Science and Engineering, Department of Mechanical and Process Engineering, Eidgenössische Technische Hochschule (ETH) Zürich, Zürich 8092, Switzerland;* orcid.org/0000-0003-4513-9682

Felix Donat − *Laboratory of Energy Science and Engineering, Department of Mechanical and Process Engineering, Eidgenössische Technische Hochschule (ETH) Zürich, Zürich 8092, Switzerland;* orcid.org/0000-0002-3940-9183

Paula M. Abdala − *Laboratory of Energy Science and Engineering, Department of Mechanical and Process Engineering, Eidgenössische Technische Hochschule (ETH) Zürich, Zürich 8092, Switzerland;* orcid.org/0000-0002-2011-1707

Complete contact information is available at: https://pubs.acs.org/10.1021/jacsau.2c00461

Notes

The authors declare no competing financial interest.

ACKNOWLEDGMENTS

This project received funding from the European Research Council under the European Union's Horizon 2020 Research and Innovation Program Grant Agreement 819573 and the Foundation Claude & Giuliana. The authors are grateful to the Scientific Center for Optical and Electron Microscopy (ScopeM) for the use of their electron microscopy facilities.

REFERENCES

(1) Canadell, J. G.; Le Quéré, C.; Raupach, M. R.; Field, C. B.; Buitenhuis, E. T.; Ciais, P.; Conway, T. J.; Gillett, N. P.; Houghton, R. A.; Marland, G. Contributions to accelerating atmospheric CO_2 growth from economic activity, carbon intensity, and efficiency of natural sinks. *Proc. Natl. Acad. Sci. U.S.A.* **2007**, *104*, 18866−18870.

(2) Bui, M.; Adjiman, C. S.; Bardow, A.; Anthony, E. J.; Boston, A.; Brown, S.; Fennell, P. S.; Fuss, S.; Galindo, A.; Hackett, L. A.; Hallett, J. P.; Herzog, H. J.; Jackson, G.; Kemper, J.; Krevor, S.; Maitland, G. C.; Matuszewski, M.; Metcalfe, I. S.; Petit, C.; Puxty, G.; Reimer, J.; Reiner, D. M.; Rubin, E. S.; Scott, S. A.; Shah, N.; Smit, B.; Trusler, J. P. M.; Webley, P.; Wilcox, J.; Mac Dowell, N. Carbon Capture and Storage (CCS): The Way Forward. *Energy Environ. Sci.* **2018**, *11*, 1062−1176.

(3) Hepburn, C.; Adlen, E.; Beddington, J.; Carter, E. A.; Fuss, S.; Mac Dowell, N.; Minx, J. C.; Smith, P.; Williams, C. K. The technological and economic prospects for CO_2 utilization and removal. *Nature* **2019**, *575*, 87−97.

(4) Rochelle, G. T. Amine Scrubbing for CO_2 Capture. *Science* **2009**, *325*, 1652−1654.

(5) Dutcher, B.; Fan, M.; Russell, A. G. Amine-Based CO_2 Capture Technology Development from the Beginning of 2013-A Review. *ACS Appl. Mater. Interfaces* **2015**, *7*, 2137−2148.

(6) Gao, W.; Liang, S.; Wang, R.; Jiang, Q.; Zhang, Y.; Zheng, Q.; Xie, B.; Toe, C. Y.; Zhu, X.; Wang, J.; Huang, L.; Gao, Y.; Wang, Z.; Jo, C.; Wang, Q.; Wang, L.; Liu, Y.; Louis, B.; Scott, J.; Roger, A. C.; Amal, R.; He, H.; Park, S. E. Industrial Carbon Dioxide Capture and Utilization: State of the Art and Future Challenges. *Chem. Soc. Rev.* **2020**, *49*, 8584−8686.

(7) Cobden, P. D.; van Beurden, P.; Reijers, H. T. J.; Elzinga, G. D.; Kluiters, S. C. A.; Dijkstra, J. W.; Jansen, D.; van den Brink, R. W. Sorption-enhanced hydrogen production for pre-combustion CO_2 capture: Thermodynamic analysis and experimental results. *Int. J. Greenh. Gas Control* **2007**, *1*, 170−179.

(8) Hanak, D. P.; Anthony, E. J.; Manovic, V. A review of developments in pilot-plant testing and modelling of calcium looping process for CO_2 capture from power generation systems. *Energy Environ. Sci.* **2015**, *8*, 2199−2249.

(9) Gouedard, C.; Picq, D.; Launay, F.; Carrette, P. L. Amine degradation in CO_2 capture. I. A review. *Int. J. Greenh. Gas Control* **2012**, *10*, 244−270.

(10) Yu, C.; Ding, J.; Wang, W.; Wei, X. Characteristics of Alkali Nitrates Molten Salt-Promoted MgO as a Moderate-Temperature CO_2 Absorbent. *Energy Proc.* **2019**, *158*, 5776−5781.

(11) Dunstan, M. T.; Donat, F.; Bork, A. H.; Grey, C. P.; Müller, C. R. CO_2 Capture at Medium to High Temperature Using Solid Oxide-Based Sorbents: Fundamental Aspects, Mechanistic Insights, and Recent Advances. *Chem. Rev.* **2021**, *121*, 12681−12745.

(12) Choi, S.; Drese, J. H.; Jones, C. W. Adsorbent Materials for Carbon Dioxide Capture from Large Anthropogenic Point Sources. *ChemSusChem* **2009**, *2*, 796−854.

(13) Kumar, S.; Saxena, S. K. A Comparative Study of CO_2 Sorption Properties for Different Oxides. *Mater. Renew. Sustain. Energy* **2014**, *3*, 30.

(14) Kierzkowska, A. M.; Pacciani, R.; Müller, C. R. CaO-Based CO_2 Sorbents: From Fundamentals to the Development of New, Highly Effective Materials. *ChemSusChem* **2013**, *6*, 1130−1148.

(15) Khatri, R. A.; Chuang, S. S. C.; Soong, Y.; Gray, M. Thermal and Chemical Stability of Regenerable Solid Amine Sorbent for CO_2 Capture. *Energy Fuel.* **2006**, *20*, 1514−1520.

(16) Dal Pozzo, A.; Armutlulu, A.; Rekhtina, M.; Abdala, P. M.; Müller, C. R. CO_2 Uptake and Cyclic Stability of MgO-Based CO_2 Sorbents Promoted with Alkali Metal Nitrates and Their Eutectic Mixtures. *ACS Appl. Energy Mater.* **2019**, *2*, 1295−1307.

(17) Gao, W.; Zhou, T.; Wang, Q. Controlled synthesis of MgO with diverse basic sites and its CO_2 capture mechanism under different adsorption conditions. *Chem. Eng. J.* **2018**, *336*, 710−720.

(18) Tan, C.; Guo, Y.; Sun, J.; Li, W.; Zhang, J.; Zhao, C.; Lu, P. Structurally improved MgO adsorbents derived from magnesium oxalate precursor for enhanced CO_2 capture. *Fuel* **2020**, *278*, 118379.

(19) Mutch, G. A.; Shulda, S.; McCue, A. J.; Menart, M. J.; Ciobanu, C. V.; Ngo, C.; Anderson, J. A.; Richards, R. M.; Vega-Maza, D. Carbon Capture by Metal Oxides: Unleashing the Potential of the (111) Facet. *J. Am. Chem. Soc.* **2018**, *140*, 4736−4742.

(20) Gregg, S. J.; Ramsay, J. D. Adsorption of Carbon Dioxide by Magnesia Studied by Use of Infrared and Isotherm Measurements. *J. Chem. Soc. A* **1970**, 2784−2787.

(21) Glasser, L.; Jenkins, H. D. B. Lattice Energies and Unit Cell Volumes of Complex Ionic Solids. *J. Am. Chem. Soc.* **2000**, *122*, 632−638.

(22) Zhang, K.; Li, X. S.; Li, W.-Z.; Rohatgi, A.; Duan, Y.; Singh, P.; Li, L.; King, D. L. Phase Transfer-Catalyzed Fast CO_2 Absorption by MgO-Based Absorbents with High Cycling Capacity. *Adv. Mater. Interfac.* **2014**, *1*, 1400030.

(23) Wang, J.; Li, G.; Li, Z.; Tang, C.; Feng, Z.; An, H.; Liu, H.; Liu, T.; Li, C. A highly selective and stable ZnO-ZrO_2 solid solution catalyst for CO_2 hydrogenation to methanol. *Sci. Adv.* **2017**, *3*, No. e1701290.

(24) Harada, T.; Simeon, F.; Hamad, E. Z.; Hatton, T. A. Alkali Metal Nitrate-Promoted High-Capacity MgO Adsorbents for Regenerable CO_2 Capture at Moderate Temperatures. *Chem. Mater.* **2015**, *27*, 1943−1949.

(25) Shkatulov, A. I.; Kim, S. T.; Miura, H.; Kato, Y.; Aristov, Y. I. Adapting the MgO-CO_2 working pair for thermochemical energy storage by doping with salts. *Energy Convers. Manag.* **2019**, *185*, 473−481.

(26) Kim, S.; Lee, K. B. Impregnation of hydrotalcite with $NaNO_3$ for enhanced high-temperature CO_2 sorption uptake. *Chem. Eng. J.* **2019**, *356*, 964−972.

(27) Bork, A. H.; Rekhtina, M.; Willinger, E.; Castro-Fernández, P.; Drnec, J.; Abdala, P. M.; Müller, C. R. Peering into buried interfaces with X-rays and electrons to unveil $MgCO_3$ formation during CO_2 capture in molten salt-promoted MgO. *Proc. Natl. Acad. Sci. U.S.A.* **2021**, *118*, No. e2103971118.

(28) Bork, A. H.; Ackerl, N.; Reuteler, J.; Jog, S.; Gut, D.; Zboray, R.; Müller, C. R. Model structures of molten salt-promoted MgO to probe the mechanism of $MgCO_3$ formation during CO_2 capture at a solid-liquid interface. *J. Mater. Chem. A* **2022**, *10*, 16803−16812.

(29) Pesce, G. L.; Fletcher, I. W.; Grant, J.; Molinari, M.; Parker, S. C.; Ball, R. J. Carbonation of Hydrous Materials at the Molecular Level: A Time of Flight-Secondary Ion Mass Spectrometry, Raman and Density Functional Theory Study. *Cryst. Growth Des.* **2017**, *17*, 1036−1044.

(30) Tan, C.; Cao, D.; Zheng, L.; Shen, Y.; Chen, L.; Chen, Y. True Reaction Sites on Discharge in Li-O_2 Batteries. *J. Am. Chem. Soc.* **2022**, *144*, 807−815.

(31) Grimaud, A.; Diaz-Morales, O.; Han, B.; Hong, W. T.; Lee, Y.-L.; Giordano, L.; Stoerzinger, K. A.; Koper, M. T. M.; Shao-Horn, Y. Activating Lattice Oxygen Redox Reactions in Metal Oxides to Catalyse Oxygen Evolution. *Nat. Chem.* **2017**, *9*, 457−465.

(32) Ascoop, I.; Galvita, V. V.; Alexopoulos, K.; Reyniers, M.-F.; Van Der Voort, P.; Bliznuk, V.; Marin, G. B. The role of CO_2 in the dehydrogenation of propane over WO_x -VO_x /SiO_2. *J. Catal.* **2016**, *335*, 1−10.

(33) Huang, Y. L.; Pellegrinelli, C.; Wachsman, E. D. Direct Observation of Oxygen Dissociation on Non-Stoichiometric Metal Oxide Catalysts. *Angew. Chem., Int. Ed.* **2016**, *55*, 15268−15271.

(34) Huang, Y.-L.; Pellegrinelli, C.; Geller, A.; Liou, S.-C.; Jarry, A.; Wang, L.; Yu, Y.; Bluhm, H.; Crumlin, E. J.; Gaskell, K. J.; Eichhorn, B. W.; Wachsman, E. D. Direct Observation of Enhanced Water and Carbon Dioxide Reactivity on Multivalent Metal Oxides and Their Composites. *Energy Environ. Sci.* **2017**, *10*, 919−923.

(35) Damaskinos, C. M.; Zavašnik, J.; Djinović, P.; Efstathiou, A. M. Dry reforming of methane over Ni/$Ce_{0.8}Ti_{0.2}O_{2-\delta}$: The effect of Ni particle size on the carbon pathways studied by transient and isotopic techniques. *Appl. Catal., B* **2021**, *296*, 120321.

https://doi.org/10.1021/jacsau.2c00461
JACS Au 2022, 2, 2731−2741

(36) Polychronopoulou, K.; AlKhoori, A. A.; Efstathiou, A. M.; Jaoude, M. A.; Damaskinos, C. M.; Baker, M. A.; Almutawa, A.; Anjum, D. H.; Vasiliades, M. A.; Belabbes, A.; Vega, L. F.; Zedan, A. F.; Hinder, S. J. Design Aspects of Doped CeO_2 for Low-Temperature Catalytic CO Oxidation: Transient Kinetics and DFT Approach. *ACS Appl. Mater. Interfaces* **2021**, *13*, 22391−22415.
(37) Gao, W.; Xiao, J.; Wang, Q.; Li, S.; Vasiliades, M. A.; Huang, L.; Gao, Y.; Jiang, Q.; Niu, Y.; Zhang, B.; Liu, Y.; He, H.; Efstathiou, A. M. Unravelling the Mechanism of Intermediate-Temperature CO_2 Interaction with Molten-$NaNO_3$ -Salt-Promoted MgO. *Adv. Mater.* **2022**, *34*, 2106677.
(38) Civiš, S.; Ferus, M.; Kubát, P.; Zukalová, M.; Kavan, L. Oxygen-Isotope Exchange between CO_2 and Solid $Ti^{18}O_2$. *J. Phys. Chem. C* **2011**, *115*, 11156−11162.
(39) Liu, P.; Abdala, P. M.; Goubert, G.; Willinger, M.; Copéret, C. Ultrathin Single Crystalline MgO(111) Nanosheets. *Angew. Chem., Int. Ed.* **2021**, *60*, 3254−3260.
(40) Knözinger, E.; Jacob, K. H.; Singh, S.; Hofmann, P. Hydroxyl Groups as IR Active Surface Probes on MgO Crystallites. *Surf. Sci.* **1993**, *290*, 388−402.
(41) Park, S. J.; Kim, Y.; Jones, C. W. $NaNO_3$ -Promoted Mesoporous MgO for High-Capacity CO_2 Capture from Simulated Flue Gas with Isothermal Regeneration. *ChemSusChem* **2020**, *13*, 2988−2995.
(42) Jo, S. I.; An, Y. I.; Kim, K. Y.; Choi, S. Y.; Kwak, J. S.; Oh, K. R.; Kwon, Y. U. Mechanisms of absorption and desorption of CO_2 by molten $NaNO_3$-promoted MgO. *Phys. Chem. Chem. Phys.* **2017**, *19*, 6224−6232.
(43) Gao, W.; Vasiliades, M. A.; Damaskinos, C. M.; Zhao, M.; Fan, W.; Wang, Q.; Reina, T. R.; Efstathiou, A. M. Molten Salt-Promoted MgO Adsorbents for CO_2 Capture: Transient Kinetic Studies. *Environ. Sci. Technol.* **2021**, *55*, 4513−4521.
(44) Tsuji, H.; Shishido, T.; Okamura, A.; Gao, Y.; Hattori, H.; Kita, H. Oxygen Exchange between Magnesium Oxide Surface and Carbon Dioxide. *J. Chem. Soc., Faraday Trans.* **1994**, *90*, 803−807.
(45) Yanagisawa, Y.; Takaoka, K.; Yamabe, S. Exchange of strong carbon dioxide O═C bonds on an MgO surface. *J. Chem. Soc., Faraday Trans.* **1994**, *90*, 2561−2566.
(46) Lara-García, H. A.; Gao, W.; Gómez-Cortés, A.; Diaz, G.; Pfeiffer, H.; Wang, Q. High and Efficient CO_2 Capture in Molten Nitrate-Modified Mg-Al-Palmitate Layered Double Oxides at High Pressures and Elucidation of Carbonation Mechanisms by in Situ DRIFT Spectroscopy Analysis. *Ind. Eng. Chem. Res.* **2019**, *58*, 5501−5509.
(47) Kust, R. N.; Duke, F. R. A Study of the Nitrate Ion Dissociation in Fused Nitrates. *J. Am. Chem. Soc.* **1963**, *85*, 3338−3340.
(48) Kust, R. N.; Burke, J. D. Thermal Decomposition in Alkali Metal Nitrate Melts. *Inorg. Nucl. Chem. Lett.* **1970**, *6*, 333−335.
(49) Nissen, D. A.; Meeker, D. E. Nitrate/Nitrite Chemistry in Sodium Nitrate-Potassium Nitrate Melts. *Inorg. Chem.* **1983**, *22*, 716−721.
(50) Bond, B. D.; Jacobs, P. W. M. The Thermal Decomposition of Sodium Nitrate. *J. Chem. Soc. A* **1966**, *60*, 1265−1268.
(51) Brooker, M. H. Kinetic Stability of Nitrate Ion in Molten Nitrate by Raman Spectroscopic Studies of ^{18}O-Enriched KNO_3. *J. Electrochem. Soc.* **1979**, *126*, 2095−2097.
(52) Luongo, G.; Donat, F.; Bork, A. H.; Willinger, E.; Landuyt, A.; Müller, C. R. Highly Selective Oxidative Dehydrogenation of Ethane to Ethylene via Chemical Looping with Oxygen Uncoupling through Structural Engineering of the Oxygen Carrier. *Adv. Energy Mater.* **2022**, *12*, 2200405.
(53) Kresse, G.; Furthmüller, J. Efficient iterative schemes forab initiototal-energy calculations using a plane-wave basis set. *Phys. Rev. B: Condens. Matter Mater. Phys.* **1996**, *54*, 11169−11186.
(54) Kresse, G.; Furthmüller, J. Efficiency of Ab-Initio Total Energy Calculations for Metals and Semiconductors Using a Plane-Wave Basis Set. *Comput. Mater. Sci.* **1996**, *6*, 15−50.
(55) Kresse, G.; Joubert, D. From Ultrasoft Pseudopotentials to the Projector Augmented-Wave Method. *Phys. Rev. B: Condens. Matter Mater. Phys.* **1999**, *59*, 1758−1775.
(56) Perdew, J. P.; Burke, K.; Ernzerhof, M. Generalized Gradient Approximation Made Simple. *Phys. Rev. Lett.* **1996**, *77*, 3865−3868.
(57) Liang, L.; Meunier, V. First-principles Raman spectra of MoS_2, WS_2 and their heterostructures. *Nanoscale* **2014**, *6*, 5394−5401.
(58) Martínez, L.; Andrade, R.; Birgin, E. G.; Martínez, J. M. PACKMOL: A Package for Building Initial Configurations for Molecular Dynamics Simulations. *J. Comput. Chem.* **2009**, *30*, 2157−2164.

https://doi.org/10.1021/jacsau.2c00461
JACS Au 2022, 2, 2731−2741